Lawrence Berkeley National Laboratory

Title
Predicting the properties of NiO with density functional theory: Impact of exchange and correlation approximations and validation of the r2SCAN functional

Permalink
https://escholarship.org/uc/item/6bq0h13j

Journal
APL Materials, 11(6)

ISSN
2166-532X

Authors
DelloStritto, Mark J
Kaplan, Aaron D
Perdew, John P
et al.

Publication Date
2023-06-01

DOI
10.1063/5.0146967

Copyright Information

Peer reviewed

Predicting the properties of NiO with density functional theory: Impact of exchange and correlation approximations and validation of the r^{2}SCAN functional

Mark J. DelloStritto,[1, a)] Aaron D. Kaplan,[2, b)] John P. Perdew,[2, 3] and Michael L. Klein[1]

[1)]*Institute for Computational Molecular Science, Temple University, Philadelphia, Pennsylvania 19122, USA*

[2)]*Department of Physics, Temple University, Philadelphia, Pennsylvania 19122, USA*

[3)]*Department of Chemistry, Temple University, Philadelphia, Pennsylvania 19122, USA*

Transition metal oxide materials are of great utility, with a diversity of topical applications ranging from catalysis to electronic devices. Because of their widespread importance in materials science, there is increasing interest in developing computational tools capable of reliable prediction of materials phase behavior and properties. The workhorse of materials theory is density functional theory (DFT). Accordingly, we have investigated the impact of various correlation and exchange approximations on their ability to predict the properties of NiO using DFT. We have chosen NiO as a particularly challenging representative of transition metal oxides in general. In so doing, we have provided a validation for use of the r^{2}SCAN density functional for predicting the materials properties of oxides. r^{2}SCAN yields accurate structural properties of NiO, and a local spin moment that notably persists under pressure, consistent with experiment. The outcome of our study is a pragmatic scheme for providing electronic structure data to enable the parameterization of interatomic potentials using state-of-the-art AI/ML methodologies. The latter are essential to allow large scale molecular dynamic simulations of bulk and surface materials phase behavior and properties with *ab initio* accuracy.

I. INTRODUCTION

The field of transition metal oxides (TMOs) covers a wide range of materials with fascinating properties and a massive array of possible structures resulting from mixtures of different transition metal elements, surface coatings, and nanostructures[1–3]. The diversity of structures of TMOs along with their favorable electronic structures make them excellent candidates for catalysis, including photocatalysts for hydrogen generation[4] and chemical synthesis[5]. It is therefore imperative that we develop accurate models of these materials, how their properties arise from the underlying electronic structure, and how they can be tuned and improved by modifying their structure and composition.

This presents significant challenges for theorists however, as the strong electron-electron interactions in these systems preclude the use of simple approximations for the electronic structure. Generalized gradient approximations (GGAs), such as the Perdew-Burke-Enzerhof (PBE) GGA, can be applied to TMOs, but only with empirical corrections such as the addition of Hubbard-like $+U$ corrections[6] or a fraction of exact exchange[7–9]. Many GGAs incorrectly predict metallic ground-states for transition metal monoxides[8]. Either correction, GGA$+U$ or exact exchange admixture, can open a gap. However, both approaches rely on tunable parameters which can negatively impact other properties of the system. For example, PBE correctly predicts the equilibrium bulk moduli and local magnetic moments of antiferromagnetic (AFM)

FeO, CoO, and NiO, but its global hybrid variants yield worse predictions of both properties[8].

An improved approach would use orbital-dependent meta-GGA functionals, as the inclusion of the local kinetic energy density can yield much more accurate models of electron correlation. The strongly constrained and appropriately normed (SCAN)[10] meta-GGA has shown great promise, as it yields an accurate and balanced description of both transition metal and main group chemistry[11]. Moreover, while SCAN often requires a $+U$ correction to accurately describe TMOs, the magnitude of the correction is significantly and systematically smaller than is needed for PBE[12,13]. However, SCAN suffers well-known numerical instabilities (see, e.g., Refs. 14–16) which limit its applicability.

Recent developments have culminated in the regularized-restored or r^{2}SCAN meta-GGA[17]. r^{2}SCAN maintains all but one of the exact physical constraints built into SCAN, and greatly improves its numeric stability, thereby greatly expanding the range of systems to which it can be applied. As with any functional, it is important to rigorously investigate its performance for a diverse array of materials.

One of the most interesting and important TMOs is NiO, a highly-insulating oxide with a rock salt structure and AFM ordering. NiO is the quintessential example of the failure of band theory due to strong electron correlation, and is the first described Mott insulator. Both paramagnetic and AFM NiO are observed to be insulating[18]. However, when local spin moments in NiO are restricted to be zero (a locally nonmagnetic and globally paramagnetic configuration) band theory and semi-local functionals predict NiO to be metallic. This is often cited as a need for explicitly-correlated methods such as dynamical mean-field theory[19]. When local (colinear) spin moments are allowed to develop on NiO formula units, an overall paramagnetic cell with a realistic gap can be obtained with GGA$+U$[18]. A similar approach using SCAN *without* a

---

[a)]Author to whom correspondence should be addressed: mark.dellostritto@temple.edu

[b)]Currently affiliated with Lawrence Berkeley National Laboratory, Berkeley, CA 94702. Author to whom correspondence should be addressed: adkaplan@lbl.govkaplan@temple.edu

+U also yielded a gap in paramagnetic NiO, albeit with a too-small gap[20]. NiO also has one of the most stable magnetic states: its Néel temperature is 525 K, and an AFM ordering persists until at least 280 GPa at room temperature[21]. NiO thus presents a vital test for any density functional applied to or any strongly correlated material.

It has been suggested[20] that NiO above its Néel temperature is not a locally-nonmagnetic insulator, but one in which there are disordered local spin moments, for which SCAN correctly finds a fundamental band gap. Thus the prediction of zero gap for a locally-nonmagnetic state by GGAs like PBE[22] and PBEsol[23] (a variant of PBE targeting the properties of solids), and by meta-GGAs like SCAN, is not necessarily wrong. We show, in the Supplementary Material, that SCAN also finds a metallic nonmagnetic ground state. PBE, PBEsol, and SCAN correctly predict an insulating AFM ground state[6], but significantly underestimate the bandgap.

Recent work[24] has shown that r^2SCAN performs comparably to SCAN for the equilibrium properties of a wide variety of TMOs. In this work, we focus on a wide range of properties for NiO, using it as a prototype of both TMOs and strongly-correlated solids. In addition, it is of interest how exact exchange admixture impacts the performance of r^2SCAN for NiO, as these corrections can significantly alter the band gap and structure of TMOs[7,8].

In this paper, we investigate the impact of exchange and correlation approximations on the structure and properties of NiO. In particular, we investigate how the PBE, PBEsol, and r^2SCAN functionals perform for NiO, and how these results are impacted by different fractions of exact exchange admixture. We are particularly interested in the equation of states predicted by each functional and how the magnetic properties are impacted. As mentioned previously, strong electron correlations give rise to a highly insulating, AFM ground state. Even small changes in interatomic distances can strongly impact the magnetic moment; in NiO, a correct description of the material requires an accurate prediction of the magnetic moment across a very wide range of temperatures and pressures.

II. COMPUTATIONAL METHODS

We computed the properties of NiO using DFT and the PBE, PBEsol, and r^2SCAN functionals via the Quantum ESPRESSO (QE) version 7.1 simulation package[25,26]. Both the PBE and PBEsol GGAs are natively implemented in QE. However, the r^2SCAN meta-GGA was accessed using LIBXC versions 5.1.5 and 5.2.2[27] (both implementations are consistent for r^2SCAN). To add exact exchange for the r^2SCAN calculations, we modified the QE code to allow for inclusion of the hybrid meta-GGA scheme. For each functional, we employed PBE optimized norm-conserving Vanderbilt (ONCV) pseudopotentials[28,29], with a plane-wave cutoff of 300 Ry and a $9 \times 9 \times 9$ $\boldsymbol{k}$-point grid. As the hybrid calculations are much more demanding, we determined, using PBE, that a 175 Ry cutoff and a $5 \times 5 \times 5$ $\boldsymbol{k}$-point grid gave converged total energies within 1 meV of those with the more-

demanding parameters. Thus the hybrids were run with this latter set of parameters. We also tested PAW pseudopotentials for PBE and PBEsol and found that the results were not significantly different (Supplementary Figs. S13 and S14). We considered rocksalt AFI, AFII, and spin-restricted (nonmagnetic) configurations of NiO. The experimentally-observed ground-state configuration of NiO is AFII[30], where ferromagnetic spins are aligned along the [111] direction of the underlying face-centered cubic unit cell[31]. The AFI solution has ferromagnetic spins aligned along the [100] direction. For a visual representation of both configurations, see Fig. S15 of the Supplementary Material. Notably, the converged solution remains AFM. The strain modulus of NiO was computed using PBE and PBEsol by optimizing the unit cell for successive strains at two percent intervals. As the stress tensor is not implemented in QE for meta-GGA functionals with spin polarization, we manually optimized the unit cell for r^2SCAN by computing the energy of NiO unit cells at 11 cubic lattice constants within $\pm 10\%$ of the experimental value, 4.171 Å[8]. The equilibrium geometry and bulk modulus were then extracted using the stabilized jellium equation of state (SJEOS)[32]. The Young's modulus and Poisson ratio were then determined by straining the system by $\pm 1\%$ in the direction transverse to the plane of magnetization (i.e. the plane formed by nearest neighbor Ni atoms with the same spin) in increments of 0.2%. For the GGA functionals, we relaxed the unit cell geometry along the unstrained lattice directions for each 0.2% increment of the strained lattice vector. For r^2SCAN, we followed a similar approach, but determined the relaxed unit cell geometry for each 0.2% increment of the strained lattice vector by varying the lengths of the unstrained lattice vectors and determining the minimum energy geometry via parabolic fit. As the meta-GGA stress tensor for spin-unrestricted systems is not yet implemented in Quantum ESPRESSO, we could not relax the cell by minimization of forces, as we did for the GGAs. For reasons of numerical stability, we have only considered global hybrids of r^2SCAN and not of SCAN.

III. RESULTS AND DISCUSSION

We present results for AFII NiO in the main text, and AFI NiO and spin-restricted NiO in the Supplementary Material. Supplementary Material Sec. S3 demonstrates that PBE, PBEsol, SCAN, and r^2SCAN all correctly place the AFII configuration as the lowest-energy configuration of NiO near the experimental lattice constant.

A. Lattice Constants and Young's Modulus

We first explore the impact of the choice of functional on the equation of state of AFII NiO. To this end, we show the energy as a function of the cubic lattice parameter in Fig. 1. There are significant differences between the results from these functionals. PBE overestimates the equilibrium lattice constant by about 0.5%, whereas PBEsol significantly underestimates it by about 1.2%. SCAN and r^2SCAN yield
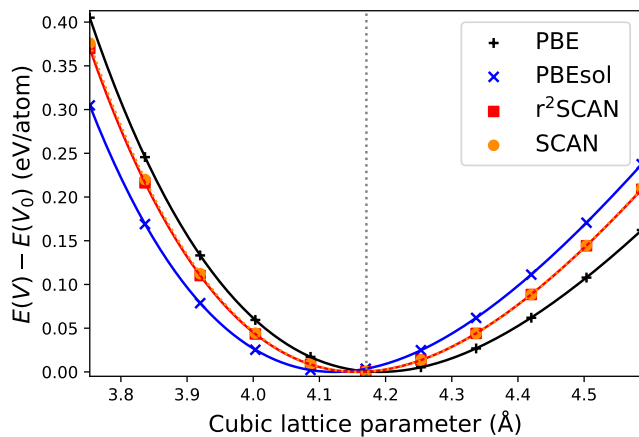
FIG. 1. Total energies (eV/atom) of AFII NiO as a function of cubic lattice constant (Å). As absolute total energies in a pseudopotential calculation have no physical meaning, all curves are plotted above their predicted minima, $E(V_0)$, with V_0 the equilibrium cell volume. The vertical dotted gray line indicates the experimental cubic lattice constant, as in Table I. The SCAN (orange circles, dotted line) and r^2SCAN (red squares, solid line) data almost coincide. Curves are the SJEOS fits.

Functional	a_0 (Å)	B_0 (GPa)	Gap (eV)
PBE	4.1910	97.2824	0.90
PBEsol	4.1223	111.2106	0.68
SCAN	4.1589	110.0333	2.64
r^2SCAN	4.1578	109.0717	2.19
Expt.	4.171	$166 - 208$	$4.0 - 4.3$

TABLE I. Comparison of AFII NiO equilibrium lattice constants a_0 (Å) and equilibrium bulk moduli B_0 (GPa) obtained by fitting to the SJEOS[32]. A variety of functionals are presented: the PBE and PBEsol GGAs; the SCAN and r^2SCAN meta-GGAs. Experimental (expt.) values for AFII NiO are taken from Ref. 8. The effects of zero-point lattice vibration have not been removed from the experimental values.

nearly exact equilibrium lattice parameters, presented in Table I, although the curvature appears to be much greater using PBEsol, SCAN, or r^2SCAN than PBE. The curvature of the energy-volume curve $E(V)$ at the equilibrium volume V_0 is typically quantified as the equilibrium bulk modulus

$$B_0 = V_0 \frac{\partial^2 E}{\partial V^2}(V_0). \tag{1}$$

Although the PBEsol GGA yields a much shorter lattice constant, it finds a nearly identical bulk modulus as r^2SCAN. This is consistent with Table XVI of Ref. 33: PBE tends to overestimate cubic lattice constants of both metals and insulators, whereas PBEsol tends to underestimate lattice constants of metals, but overestimate lattice constants of insulators less than PBE. Note, however, that PBEsol exceeds the accuracy of both SCAN and r^2SCAN in predicting the absolute magnetization of pure ferromagnetic Ni metal[33].

To further investigate the differences in the equation of state, we also show the absolute magnetization of one Ni atom
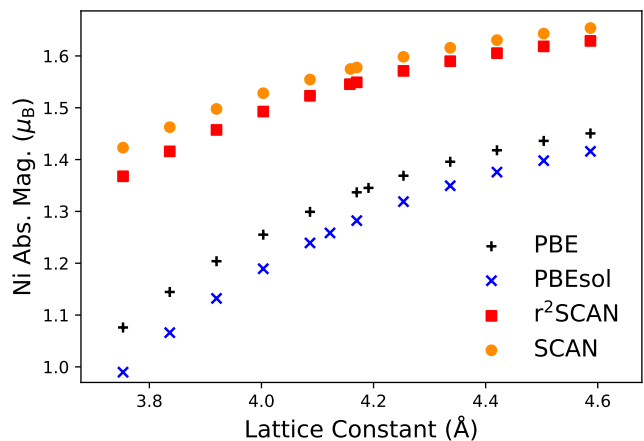
FIG. 2. Absolute value of the magnetic moment of a Ni atom, in units of the Bohr magneton μ_B, as a function of lattice constant (Å) for PBE, PBEsol, SCAN, and r^2SCAN.

in Fig. 2. While the energy as a function of lattice constant varies slightly between each functional, in Fig. 2, we see a much larger difference in the magnetization between r^2SCAN and the GGAs, particularly at smaller lattice constants or, analogously, higher pressures. While the PBE and PBEsol GGAs exhibit a large collapse in magnetization at shorter lattice constants, SCAN and r^2SCAN show less variation in the absolute magnetization across the range of lattice constants tested. Importantly, r^2SCAN thus appears to yield not only a more accurate lattice constant compared to experiment, but it also appears to yield a more accurate magnetization as a function of pressure. Indeed, compared to GGA functionals, r^2SCAN exhibits an improvement in the magnetization as a function of pressure similar to that of hybrid functionals.[34] Experiments have shown that the AFM state of NiO is remarkably stable with regards to compression, with AFM ordering persisting to at least 280 GPa[21]. r^2SCAN is the only tested functional that matches this behavior.

The rapid collapse of the magnetic moment predicted by PBE and PBEsol may be indicative of nearly degenerate spin states which compete with the AFII configuration. Indeed, Supplementary Figs. S4 and S5 demonstrate that both PBE and PBEsol make AFI and paramagnetic NiO degenerate in energy for lattice constants shorter than the experimental value, and nearly degenerate for longer lattice constants. Supplementary Figs. S6 and S7 show that the AFI, AFII, and paramagnetic configurations of SCAN and r^2SCAN are sufficiently well-separated not to compete in energy for the range of lattice constants considered here.

Note that all three functionals, PBE, PBEsol, and r^2SCAN, predict a non-vanishing magnetization for AFII NiO at lattice constants within $(\pm 10)\%$ of the experimental value. All three predict the magnetization to rise monotonically with increasing lattice constants. However, it is clear that r^2SCAN more reliably predicts the properties of NiO across magnetic phases.

The differences exhibited by the functionals in the curvature of the energy as a function of the lattice constant suggest that the predicted mechanical properties of NiO will also dif-

fer significantly. Thus, in addition to computing the bulk modulus of NiO, we have computed the Young's modulus of AFI NiO with each functional. For reasons of computational complexity, we perform the computation of the Young's modulus only for the AFI configuration of NiO, where the magnetization aligns with a conventional lattice vector. We compute the Young's modulus perpendicular to the plane formed by the alternating Ni spins, such that the system is strained in the same direction as the magnetization. The Young's modulus of AFI NiO is 155.4 GPa computed with PBE; 168.7 GPa with PBEsol; and 325.8 GPa with r^2SCAN. As expected, there is a very large variance in the modulus for each functional, with the r^2SCAN prediction more than double the PBE result, matching the large differences for the bulk moduli in Table I. Thus, while the bulk moduli of PBE, SCAN, and r^2SCAN are fairly close in value, the components of the stress tensor can exhibit much larger differences.

B. Band Gap and Magnetization

We now investigate the impact of exact exchange admixture on the electronic properties of NiO, and how this differs for GGA and meta-GGA functionals. Exact exchange admixture is often necessary to yield quantitatively accurate band gaps and, at least at the GGA level, the correct structures of solids, liquids, interfaces, and molecules. However, the needed fraction of exact exchange is system- and property-dependent: large exchange fractions can improve band positions while negatively impacting other properties of the system, such as the molecular dipole moment and polarizability[35,36].

Accordingly, we investigated the impact of exact exchange admixture on the band gap and absolute magnetization of NiO by generating global hybrids of PBE and r^2SCAN, varying the fraction from 0 to 0.5 in increments of 0.05. The global hybrids were evaluated at the equilibrium lattice constants of the parent functional in Table I. The band gap is plotted as a function of the exchange fraction in Fig. 3(A), along with the corresponding valence band maximum (VBM) and conduction band minimum (CBM) in Fig. 3(B). As expected, adding only 5% exact exchange to PBE opens a band gap in AFI NiO, although even at large fractions, PBE systematically predicts smaller band gaps compared to r^2SCAN. Indeed, to get within the experimental range of the NiO band gap[8,9] (3.7-4.3 eV), one needs 20-25% exact exchange for r^2SCAN, but 30-35% for PBE. Interestingly, while the magnitudes of the shifts in the band edges with exact-exchange fraction are about equal in PBE, they are much bigger for the valence band edge in r^2SCAN.

Underestimation of the bandgap is theoretically understood as the lack of a derivative discontinuity in standard Kohn-Sham DFT[37] and approximate pure-density functionals, such as GGAs. Orbital-dependent functionals, such as meta-GGAs or hybrid functionals, when implemented in a generalized Kohn-Sham scheme (as is done in Quantum ESPRESSO), can yield an exchange-correlation potential that is not just a function of position, and thus larger bandgaps[38–40]. See Ref. 33 for further discussion.

(a)

(b)
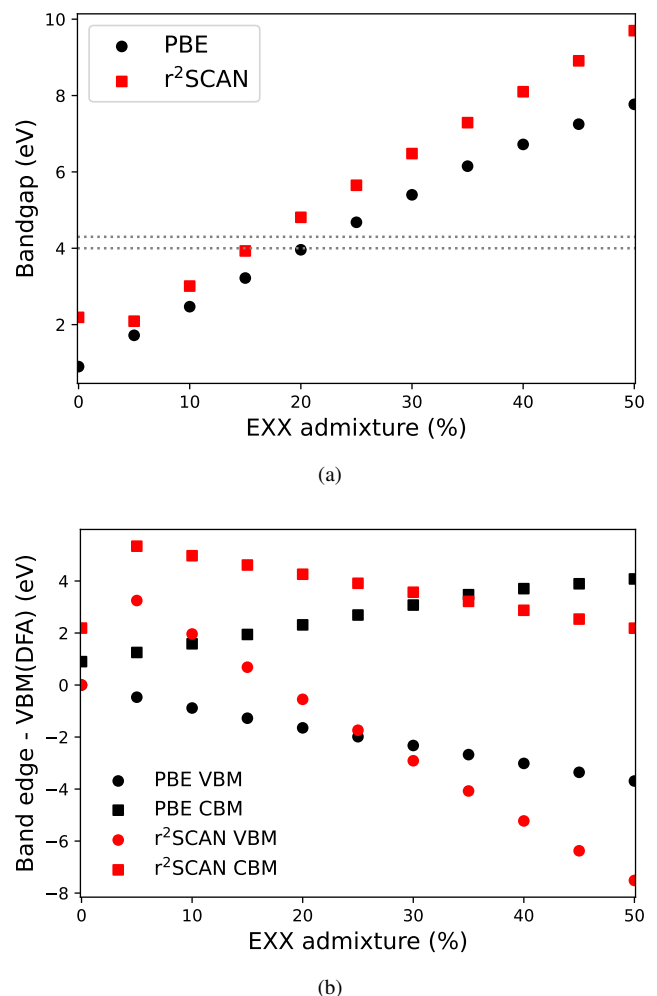
FIG. 3. (a) Band gap or (b) band edges: the valence band maximum (VBM) (filled circles) and conduction band minimum (CBM or cb) (filled squares) for AFII NiO, using global hybrids of PBE and r^2SCAN, as a function of exact exchange fraction. VBM(DFA) is calculated for 0% exact exchange. Both the band gap and band edges are given in eV. For analogous plots of the AFI configuration of NiO, see Supplementary Figs. S10 and S11. The dotted horizontal lines in panel (a) indicate the range of experimental values of the band gap.

Notably, the exact exchange admixture also has a large impact on the absolute magnetization of the Ni atoms (Fig. 4), with increasing fractions of exact exchange increasing the magnetic moment of the Ni atoms such that they approach the experimental value 1.90 μ_B[9]. Once again, the PBE values are systematically smaller than the r^2SCAN values, especially at zero exact exchange fraction.

Moving from a meta-GGA to a hybrid meta-GGA does not impact the r^2SCAN magnetic moments very strongly: the 5% r^2SCAN hybrid has a lower magnetic moment than r^2SCAN. For PBE, there is a large jump in the magnetic moment at 5% exact exchange admixture, followed by much smaller changes with increasing exact exchange fraction. This finding is likely due to the gap widening in the PBE case, and thus high-
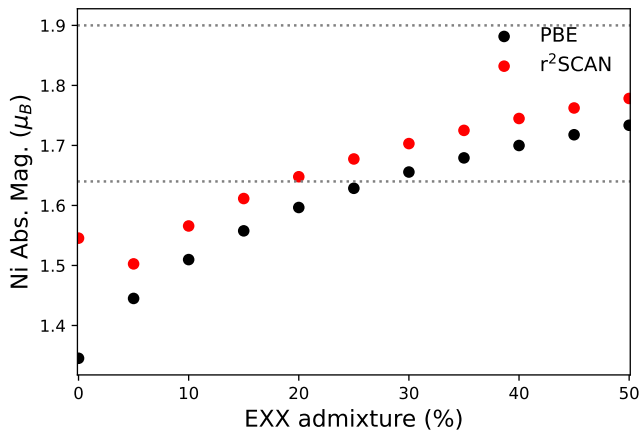
FIG. 4. Magnetization of Ni atom in AFII NiO as a function of exact exchange fraction, using global hybrids of PBE and r²SCAN. For an analogous plot of the AFI configuration of NiO, see Supplementary Fig. S12. The dotted horizontal lines indicate the range of experimental values.

lights the improved description of electronic correlation associated with r²SCAN. This observation also helps explain the observed discrepancy between either PBE or PBEsol and r²SCAN in Fig. 2, where both PBE and PBEsol severely underestimate the AFII NiO bandgap at the minimum energy structure. One expects a small or zero gap for NiO at very high pressures, where there is a transition to a paramagnetic phase. On the other hand, r²SCAN correctly predicts an insulating state due to the better description of electronic correlation across a wide range of NiO geometries, thereby preserving an AFM ordering under large hydrostatic compression.

IV. CONCLUSIONS

In this work, we have investigated the influence of exchange and correlation approximations on the computed properties of NiO, especially its electronic, mechanical, and magnetic properties. While all functionals predict similar antiferromagnetic ground-state structures for NiO, they differ strongly in the response of the energy and magnetic moment to perturbations of the structure. While it is expected that the absolute magnetization of NiO is robust to changes in its structure, the PBE and PBEsol GGAs predict a rapid collapse of the magnetization with even modest reductions in the lattice constant. Only the r²SCAN meta-GGA correctly predicts an essentially constant magnetization over the range of lattice constants studied. Similarly, r²SCAN predicts significantly different mechanical properties, combining a similar lattice constant to that of PBE but with larger elastic moduli, which more closely match the predictions of PBEsol.

Notably, we still find that it is necessary to add 20-25% exact exchange to reproduce the experimental band gaps, which matches behavior for other oxide systems[7–9]. Just as meta-GGAs tend to require smaller Hubbard-like $+U$ corrections than GGAs to accurately describe transition metal oxides[12],

r²SCAN requires a smaller fraction of exact exchange than PBE to yield a quantitatively correct bandgap. The improved description of electron correlation in r²SCAN leads to a lesser impact of exchange fraction on both the band gap and magnetization.

Overall, we find that r²SCAN yields excellent results for NiO across a wide range of range of lattice constants. Moreover, it qualitatively matches experimental results for different properties. Accordingly, we recommend its use in generating data to fit interatomic potentials with the now popular AI/ML methodologies, which in turn enable large scale molecular dynamics computations at *ab initio* accuracy[41,42].

V. SUPPLEMENTARY MATERIAL

Supplementary material is provided online including convergence tests for the functionals, elaboration on the equation of state fitting procedure, equations of state for AFI and nonmagnetic NiO, the magnetic properties of AFI NiO, comparison of ONCV and PAW pseudopotentials, and illustrations of the AFI and AFII NiO.

ACKNOWLEDGMENTS

[1] M. A. Peña and J. L. G. Fierro, "Chemical structures and performance of perovskite oxides," Chem. Rev. **101**, 1981–2018 (2001).

[2] R. B. Comizzoli, R. P. Frankenthal, P. C. Milner, and J. D. Sinclair, "Corrosion of electronic materials and devices," Science **234**, 340–345 (1986).

[3] N. Basavegowda, K. Mishra, and Y. R. Lee, "Synthesis, characterization, and catalytic applications of hematite (α-Fe$_2$O$_3$) nanoparticles as reusable nanocatalyst," Adv. Nat. Sci: Nanosci. Nanotechnol. **8**, 025017 (2017).

[4] M. Pelaez, N. T. Nolan, S. C. Pillai, M. K. Seery, P. Falaras, A. G. Kontos, P. S. Dunlop, J. W. Hamilton, J. Byrne, K. O'Shea, M. H. Entezari, and D. D. Dionysiou, "A review on the visible light active titanium dioxide photocatalysts for environmental applications," Appl. Catal. B: Environ. **125**, 331–349 (2012).

[5] J. C. Védrine, "Heterogeneous catalysis on metal oxides," Catalysts **7**, 341 (2017).

[6] H. Peng and J. P. Perdew, "Synergy of van der Waals and self-interaction corrections in transition metal monoxides," Phys. Rev. B **96**, 100101 (2017).

[7] I. de P. R. Moreira, F. Illas, and R. L. Martin, "Effect of fock exchange on the electronic structure and magnetic coupling in nio," Phys. Rev. B **65**, 155102 (2002).

[8] F. Tran, P. Blaha, K. Schwarz, and P. Novák, "Hybrid exchange-correlation energy functionals for strongly correlated electrons: Applications to transition-metal monoxides," Phys. Rev. B **74**, 155108 (2006).

[9] C. Rödl, F. Fuchs, J. Furthmüller, and F. Bechstedt, "Quasiparticle band structures of the antiferromagnetic transition-metal oxides MnO, FeO, CoO, and NiO," Phys. Rev. B **79**, 235114 (2009).

[10] J. Sun, A. Ruzsinszky, and J. P. Perdew, "Strongly constrained and appropriately normed semilocal density functional," Phys. Rev. Lett. **115**, 036402 (2015).

[11] J. G. Brandenburg, J. E. Bates, J. Sun, and J. P. Perdew, "Benchmark tests of a strongly constrained semilocal functional with a long-range dispersion correction," Phys. Rev. B **94**, 115144 (2016).

[12] G. Sai Gautam and E. A. Carter, "Evaluating transition metal oxides within DFT-SCAN and SCAN $+ U$ frameworks for solar thermochemical applications," Phys. Rev. Mater. **2**, 095401 (2018).

[13] O. Y. Long, G. Sai Gautam, and E. A. Carter, "Evaluating optimal U for $3d$ transition-metal oxides within the SCAN+U framework," Physical Review Materials **4**, 045401 (2020), publisher: American Physical Society.

[14] Z.-h. Yang, H. Peng, J. Sun, and J. P. Perdew, "More realistic band gaps from meta-generalized gradient approximations: Only in a generalized Kohn-Sham scheme," Phys. Rev. B **93**, 205205 (2016).

[15] Y. Yamamoto, C. M. Diaz, L. Basurto, K. A. Jackson, T. Baruah, and R. R. Zope, "Fermi-Löwdin orbital self-interaction correction using the strongly constrained and appropriately normed meta-GGA functional," J. Chem. Phys. **151**, 154105 (2019).

[16] A. P. Bartók and J. R. Yates, "Regularized SCAN functional," J. Chem. Phys. **150**, 161101 (2019).

[17] J. W. Furness, A. D. Kaplan, J. Ning, J. P. Perdew, and J. Sun, "Accurate and numerically efficient r²SCAN meta-generalized gradient approximation," J. Phys. Chem. Lett. **11**, 8208–8215 (2020), correction, *ibid.* **11**, 9248 (2020).

[18] G. Trimarchi, Z. Wang, and A. Zunger, "Polymorphous band structure model of gapping in the antiferromagnetic and paramagnetic phases of the Mott insulators MnO, FeO, CoO, and NiO," Phys. Rev. B **97**, 035107 (2018).

[19] S. Choi, A. Kutepov, K. Haule, M. van Schilfgaarde, and G. Kotliar, "First-principles treatment of mott insulators: linearized qsgw+dmft approach," npj Quant. Mater. **1**, 16001 (2016).

[20] Y. Zhang, J. Furness, R. Zhang, Z. Wang, A. Zunger, and J. Sun, "Symmetry-breaking polymorphous descriptions for correlated materials without interelectronic U," Phys. Rev. B **102**, 045112 (2020).

[21] V. Potapkin, L. Dubrovinsky, I. Sergueev, M. Ekholm, I. Kantor, D. Bessas, E. Bykova, V. Prakapenka, R. P. Hermann, R. Rüffer, V. Cerantola, H. J. M. Jönsson, W. Olovsson, S. Mankovsky, H. Ebert, and I. A. Abrikosov, "Magnetic interactions in nio at ultrahigh pressure," Phys. Rev. B **93**, 201110 (2016).

[22] J. P. Perdew, K. Burke, and M. Ernzerhof, "Generalized gradient approximation made simple," Phys. Rev. Lett. **77**, 3865 (1996).

[23] J. P. Perdew, A. Ruzsinszky, G. I. Csonka, O. A. Vydrov, G. E. Scuseria, L. A. Constantin, X. Zhou, and K. Burke, "Restoring the density-gradient expansion for exchange in solids and surfaces," Phys. Rev. Lett. **100**, 136406 (2008).

[24] S. Swathilakshmi, R. Devi, and G. S. Gautam, "Performance of the r²SCAN functional in transition metal oxides," (2023), arXiv:2301.00535.

[25] P. Giannozzi, S. Baroni, N. Bonini, M. Calandra, R. Car, C. Cavazzoni, D. Ceresoli, G. L. Chiarotti, M. Cococcioni, I. Dabo, A. D. Corso, S. de Gironcoli, S. Fabris, G. Fratesi, R. Gebauer, U. Gerstmann, C. Gougoussis, A. Kokalj, M. Lazzeri, L. Martin-Samos, N. Marzari, F. Mauri, R. Mazzarello, S. Paolini, A. Pasquarello, L. Paulatto, C. Sbraccia, S. Scandolo, G. Sclauzero, A. P. Seitsonen, A. Smogunov, P. Umari, and R. M. Wentzcovitch, "QUANTUM ESPRESSO: a modular and open-source software project for quantum simulations of materials," J. Phys. Condens. Matter **21**, 395502 (2009).

[26] P. Giannozzi, O. Andreussi, T. Brumme, O. Bunau, M. B. Nardelli, M. Calandra, R. Car, C. Cavazzoni, D. Ceresoli, M. Cococcioni, N. Colonna, I. Carnimeo, A. D. Corso, S. de Gironcoli, P. Delugas, R. A. DiStasio, A. Ferretti, A. Floris, G. Fratesi, G. Fugallo, R. Gebauer, U. Gerstmann, F. Giustino, T. Gorni, J. Jia, M. Kawamura, H.-Y. Ko, A. Kokalj, E. Küçükbenli, M. Lazzeri, M. Marsili, N. Marzari, F. Mauri, N. L. Nguyen, H.-V. Nguyen, A. O. de-la Roza, L. Paulatto, S. Poncé, D. Rocca, R. Sabatini, B. Santra, M. Schlipf, A. P. Seitsonen, A. Smogunov, I. Timrov, T. Thonhauser, P. Umari, N. Vast, X. Wu, and S. Baroni, "Advanced capabilities for materials modelling with Quantum ESPRESSO," J. Phys. Condens. Matter **29**, 465901 (2017).

[27] S. Lehtola, C. Steigemann, M. J. Oliveira, and M. A. Marques, "Recent developments in LIBXC — a comprehensive library of functionals for density functional theory," SoftwareX **7**, 1–5 (2018).

[28] D. Vanderbilt, "Optimally smooth norm-conserving pseudopotentials," Phys. Rev. B **32**, 8412–8415 (1985).

[29] M. Schlipf and F. Gygi, "Optimization algorithm for the generation of oncv pseudopotentials," Computer Phys. Commun. **196**, 36–44 (2015).

[30] W. L. Roth and G. A. Slack, "Antiferromagnetic structure and domains in single crystal nio," J. Appl. Phys. **31**, S352–S353 (1960).

[31] A. Schrön, C. Rödl, and F. Bechstedt, "Energetic stability and magnetic properties of MnO in the rocksalt, wurtzite, and zinc-blende structures: Influence of exchange and correlation," Phys. Rev. B **82**, 165109 (2010).

[32] A. B. Alchagirov, J. P. Perdew, J. C. Boettger, R. C. Albers, and C. Fiolhais, "Energy and pressure versus volume: Equations of state motivated by the stabilized jellium model," Phys. Rev. B **63**, 2241151–22411516 (2001).

[33] A. D. Kaplan and J. P. Perdew, "Laplacian-level meta-generalized gradient approximation for solid and liquid metals," Phys. Rev. Materials **6**, 083803 (2022).

[34] X.-B. Feng and N. M. Harrison, "Metal-insulator and magnetic transition of NiO at high pressures," Physical Review B **69**, 035114 (2004), publisher: American Physical Society.

[35] D. Hait and M. Head-Gordon, "How accurate is density functional theory at predicting dipole moments? An assessment using a new database of 200 benchmark values," J. Chem. Theory Comput. **14**, 1969–1981 (2018).

[36] M. DelloStritto, J. Xu, X. Wu, and M. L. Klein, "Aqueous solvation of the chloride ion revisited with density functional theory: impact of correlation and exchange approximations," Phys. Chem. Chem. Phys. **22**, 10666–10675 (2020).

[37] J. P. Perdew, W. Yang, K. Burke, Z. Yang, E. K. Gross, M. Scheffler, G. E. Scuseria, T. M. Henderson, I. Y. Zhang, A. Ruzsinszky, H. Peng, J. Sun, E. Trushin, and A. Görling, "Understanding band gaps of solids in generalized Kohn-Sham theory," Proc. Nat. Acad. Sci. U.S.A. **114**, 2801–2806 (2017).

[38] N. M. Harrison, V. R. Saunders, R. Dovesi, W. C. Mackrodt, A. S. Alexandrov, C. N. R. Rao, J. N. Murrell, R. L. Johnston, and D. E. Logan, "Transition Metal Materials: A First Principles Approach to the Electronic Structure of the Insulating Phase [and Discussion]," Philosophical Transactions: Mathematical, Physical and Engineering Sciences **356**, 75–88 (1998), publisher: The Royal Society.

[39] M. D. Towler, N. L. Allan, N. M. Harrison, V. R. Saunders, W. C. Mackrodt, and E. Aprà, "Ab initio study of MnO and NiO," Physical Review B **50**, 5041–5054 (1994), publisher: American Physical Society.

[40] J. Muscat, A. Wander, and N. M. Harrison, "On the prediction of band gaps from hybrid functional theory," Chemical Physics Letters **342**, 397–401 (2001).

[41] L. Zhang, J. Han, H. Wang, R. Car, and W. E, "Deep potential molecular dynamics: A scalable model with the accuracy of quantum mechanics," Phys. Rev. Lett. **120**, 143001 (2018).

[42] C. Malosso, L. Zhang, R. Car, S. Baroni, and D. Tisi, "Viscosity in water from first-principles and deep-neural-network simulations," npj Comput. Mater. **8**, 139 (2022).

[43] C. R. Harris, K. J. Millman, S. J. van der Walt, R. Gommers, P. Virtanen, D. Cournapeau, E. Wieser, J. Taylor, S. Berg, N. J. Smith, R. Kern, M. Picus, S. Hoyer, M. H. van Kerkwijk, M. Brett, A. Haldane, J. F. del Río, M. Wiebe, P. Peterson, P. Gérard-Marchant, K. Sheppard, T. Reddy, W. Weckesser, H. Abbasi, C. Gohlke, and T. E. Oliphant, "Array programming with NumPy," Nature **585**, 357–362 (2020).

[44] R. M. Hanson, J. Prilusky, Z. Renjian, T. Nakane, and J. L. Sussman, "JSmol and the Next-Generation Web-Based Representation of 3D Molecular Structure as Applied to Proteopedia," Isr. J. Chem. **53**, 207–216 (2013).

FIG. S5. Convergence of the PBE total energy of AFI NiO with respect to $\boldsymbol{k}$-point density and plane-wave energy cutoff. Each different set of colored points represents a $\boldsymbol{k}$-point density, with N_k points per axis. The horizontal axis represents the plane-wave energy cutoff $\varepsilon_{\mathrm{cut}}$. The vertical axis presents the absolute deviation of the total energy, $E(N_k, \varepsilon_{\mathrm{cut}})$ from the "well-converged" total energy computed with the densest $\boldsymbol{k}$-point grid (11 points/axis) and highest plane-wave cutoff (400 Ry).

SUPPLEMENTARY MATERIAL:
PREDICTING THE PROPERTIES OF NIO WITH DENSITY
FUNCTIONAL THEORY: IMPACT OF EXCHANGE AND
CORRELATION APPROXIMATIONS AND VALIDATION OF
THE R^{2}SCAN FUNCTIONAL

CONTENTS

S6. CONVERGENCE TESTING

To ensure well-converged results, we studied the convergence of the PBE total energy of NiO using different sets of $\boldsymbol{k}$-points and plane-wave energy cutoffs. We used uniform $\boldsymbol{k}$-point grids with equal numbers of points per axis (e.g., $9 \times 9 \times 9$) due to the cubic symmetry of NiO. Therefore we considered five $\boldsymbol{k}$-grids with either 3, 5, 7, 9, or 11 $\boldsymbol{k}$-points per axis, and energy cutoffs in the range 40 Ry to 400 Ry. The results of this test are shown in Fig. S5.

S7. EQUATION OF STATE FITTING

To obtain optimized geometries for NiO, we performed a series of single-point total energy calculations with the tetrahedron method, as outlined in the main text. These energies were then fitted to a model equation of state, here selected to be the stabilized jellium equation of state (SJEOS)[32]

$$E(V) = \alpha \left(\frac{V_0}{V}\right) + \beta \left(\frac{V_0}{V}\right)^{2/3} + \gamma \left(\frac{V_0}{V}\right)^{1/3} + \omega. \tag{S2}$$

V_0 is then the equilibrium volume, such that the hydrostatic pressure on the cell vanishes,

$$P(V_0) = -\frac{\partial E}{\partial V}(V_0) = 0. \tag{S3}$$

One can perform a simple least-squares fit, as we did using the `lstsq` function of NumPy's `linalg` library[43], to the coefficients $V_0\alpha$, $V_0^{2/3}\beta$, $V_0^{1/3}\gamma$, and ω. The bulk moduli are then easily computed as

$$B(V) = V\frac{\partial^2 E}{\partial V^2} = \frac{1}{9V}\left[18\alpha\left(\frac{V_0}{V}\right) + 10\beta\left(\frac{V_0}{V}\right)^{2/3} + 4\gamma\left(\frac{V_0}{V}\right)^{1/3}\right]. \tag{S4}$$

Also occasionally of interest is the first derivative of the bulk modulus with respect to pressure,

$$B_1(V) = \frac{\partial B}{\partial P} = -\frac{1}{B(V)}\left[B(V) + V^2\frac{\partial^3 E}{\partial V^3}\right] \tag{S5}$$

$$= \frac{1}{27VB(V)}\left[108\alpha\left(\frac{V_0}{V}\right) + 50\beta\left(\frac{V_0}{V}\right)^{2/3} + 16\gamma\left(\frac{V_0}{V}\right)^{1/3}\right]. \tag{S6}$$

A summary of the SJEOS fitted parameters and equilibrium properties of AFI NiO is given in Table S3. Note that the coefficient of determination, which gauges the quality of fit, is given as

$$R^2 = 1 - \left\{\sum_{i=1}^{N_V}\left[E_{\text{calc}}(V_i) - E_{\text{SJEOS}}(V_i)\right]^2\right\}\left\{\sum_{i=1}^{N_V}\left[E_{\text{calc}}(V_i) - \overline{E}_{\text{calc}}\right]^2\right\}^{-1}, \tag{S7}$$

$$\overline{E}_{\text{calc}} = \frac{1}{N_V}\sum_{i=1}^{N_V}E_{\text{calc}}(V_i). \tag{S8}$$

In those equations, the sums run over N_V single-point calculated energies $E_{\text{calc}}(V)$; $E_{\text{SJEOS}}(V)$ are the energies calculated using Eq. S2.

Functional	α (Ry)	β (Ry)	γ (Ry)	ω (Ry)	E_0 (Ry/atom)	V_0 (Å^3)	a_0 (Å)	B_0 (GPa)	$B_1(V_0)$	Gap (eV)	R^2
PBE	11.554025	-27.270480	19.878884	-344.368377	-85.051487	36.806323	4.1910	97.282409	4.563130	0.90	0.999999
PBEsol	12.251403	-28.712831	20.671452	-343.984221	-84.943549	35.027005	4.1223	111.210563	4.523545	0.68	0.999998
SCAN	11.752940	-27.088733	18.918644	-343.809066	-85.056554	35.968393	4.1589	110.033331	4.438533	2.64	0.999996
r^{2}SCAN	11.602760	-26.716261	18.624242	-343.783145	-85.068101	35.938781	4.1578	109.071707	4.433852	2.19	0.999998

TABLE S2. Parameters used in the SJEOS of Eq. S2 (all Ry), and the deduced equilibrium volume V_0 (Å^3) and associated cubic lattice constant a_0 (Å) of AFII NiO. This configuration is experimentally determined to be the ground-state. $E_0 = E(V_0)$ is the total energy at the equilibrium volume, which can be compared to the other magnetic configurations of NiO to deduce the ground-state. Also shown are the equilibrium bulk modulus, $B_0 \equiv B(V_0)$ (GPa) using Eq. S4, and its first derivative with respect to pressure, $B_1(V_0)$ (dimensionless), using Eq. S6. Last, we show the quality of the fit (coefficient of determination), defined in Eq. S7.

A. AFI NiO

While the ground-state of NiO is experimentally determined to be the AFII configuration, the AFI configuration lies close in energy. Table S3 presents SJEOS fit parameters and extrapolated equilibrium properties of the AFII configuration of NiO. Figure S6 plots the SJEOS fits alongside the computed total energies as a function of cubic lattice constant.
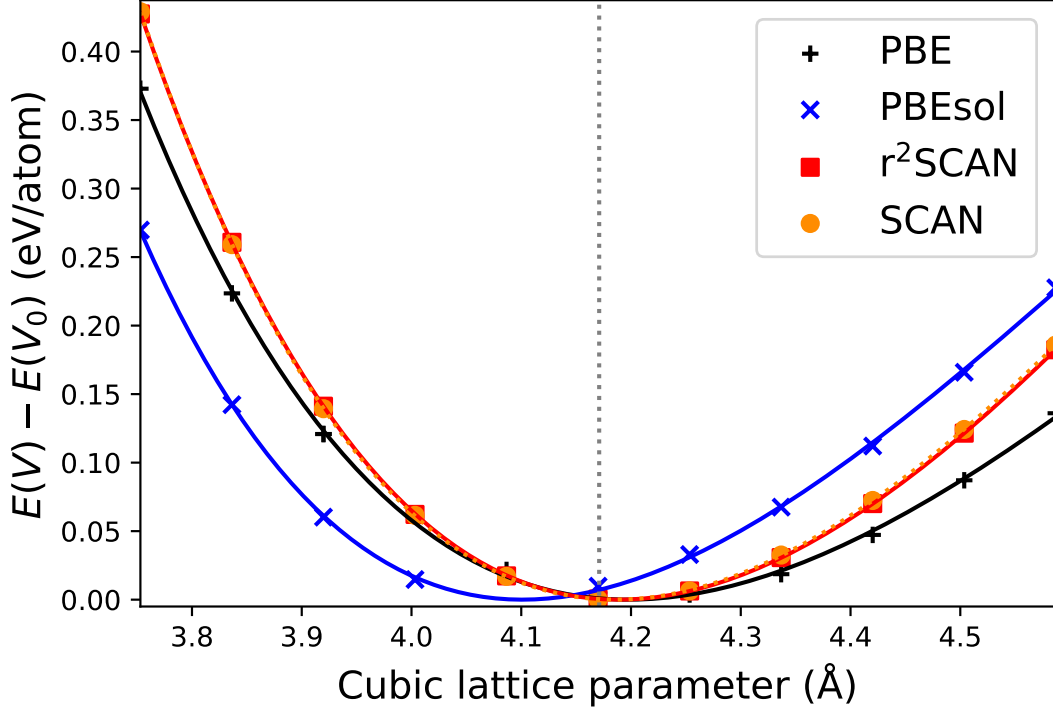
FIG. S6. Total energies of AFI NiO as a function of lattice constant. Dashed lines are SJEOS fits using the parameters in Table S3. All energies are plotted relative to the energy at the equilibrium volume V_0. The vertical, gray dotted line indicates the experimental equilibrium lattice constant, 4.171 Å[8].

Functional	α (Ry)	β (Ry)	γ (Ry)	ω (Ry)	E_0 (Ry/atom)	V_0 (Å³)	a_0 (Å)	B_0 (GPa)	$B_1(V_0)$	Gap (eV)	R^2
PBE	22.799316	-55.585932	42.773917	-690.356145	-85.046106	73.964030	4.1977	167.820661	4.779526	0.00	0.999336
PBEsol	33.393948	-84.852596	69.523347	-697.576690	-84.938999	68.960930	4.1008	215.360633	5.178446	0.00	0.999553
SCAN	23.501798	-54.205036	37.904679	-687.625920	-85.053060	73.312127	4.1853	215.411987	4.441796	1.17	0.999994
r²SCAN	21.887340	-49.531502	33.400982	-686.269772	-85.064119	73.487421	4.1886	212.659064	4.356890	0.76	0.999994

TABLE S3. Parameters used in the SJEOS of Eq. S2 (all Ry), and the deduced equilibrium volume V_0 (Å³) and associated cubic lattice constant a_0 (Å) of AFI NiO. $E_0 = E(V_0)$ is the total energy at the equilibrium volume, which can be compared to the other magnetic configurations of NiO to deduce the ground-state. Also shown are the equilibrium bulk modulus, $B_0 \equiv B(V_0)$ (GPa) using Eq. S4, and its first derivative with respect to pressure, $B_1(V_0)$ (dimensionless), using Eq. S6. Last, we show the quality of the fit (coefficient of determination), defined in Eq. S7.

B. Nonmagnetic NiO

As is commonly done, we performed spin-restricted calculations of NiO, which assume that the local moments on Ni and O are identically zero (locally nonmagnetic, sometimes called paramagnetic). Table S4 presents the SJEOS fit parameters and extrapolated equilibrium properties of nonmagnetic NiO. Figure S7 plots the SJEOS fits alongside the computed total energies as a function of cubic lattice constant.
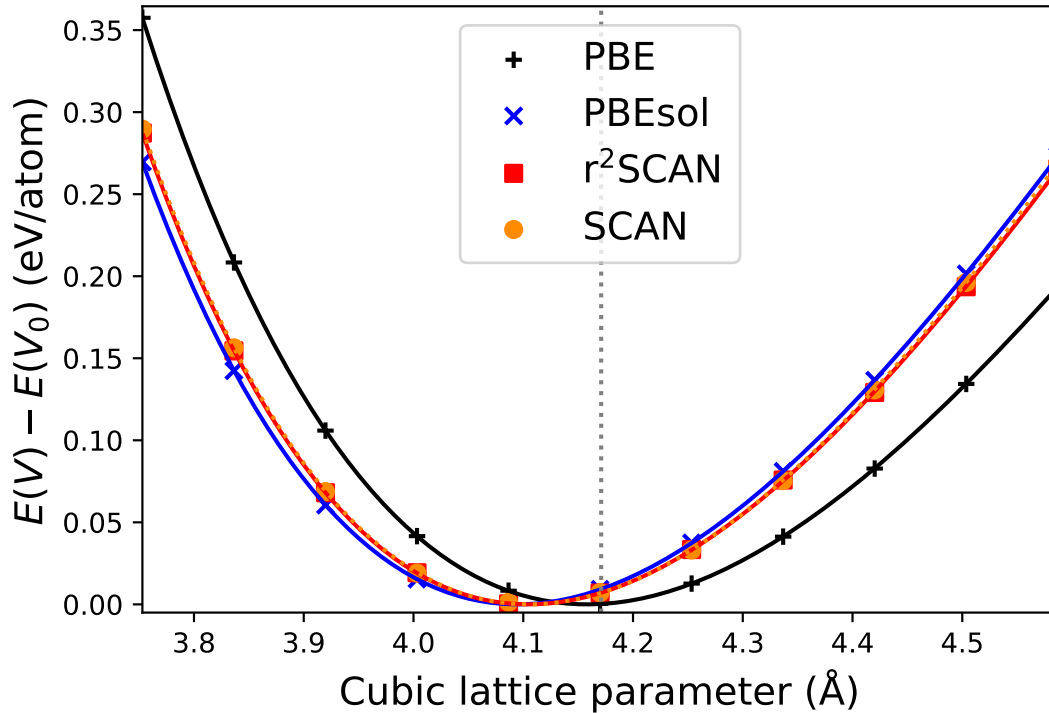
FIG. S7. Total energies of spin-restricted NiO as a function of lattice constant. Dashed lines are SJEOS fits using the parameters in Table S4. All energies are plotted relative to the energy at the equilibrium volume V_0. The vertical, gray dotted line indicates the experimental AFII equilibrium lattice constant, 4.171 Å[8].

Functional	α (Ry)	β (Ry)	γ (Ry)	ω (Ry)	E_0 (Ry/atom)	V_0 (Å^3)	a_0 (Å)	B_0 (GPa)	$B_1(V_0)$	Gap (eV)	R^2
PBE	6.220216	-14.824204	10.987760	-172.473632	-85.044930	17.973781	4.1581	103.396991	4.621350	0.00	0.999999
PBEsol	6.536526	-15.423517	11.237454	-172.228351	-84.938944	17.162343	4.0946	118.153798	4.561498	0.00	0.999998
SCAN	6.279822	-14.598797	10.358127	-172.094273	-85.027560	17.296601	4.1053	118.766020	4.480856	0.00	0.999989
r^{2}SCAN	6.483209	-15.245693	11.041760	-172.379609	-85.050167	17.287071	4.1045	117.802078	4.542177	0.00	0.999988

TABLE S4. SJEOS fit parameters and extracted equilibrium properties of spin-restricted NiO. This configuration has zero magnetic moment on each atomic site.

S8. RELATIVE PHASE ORDERING

Figures S8–S11 plot the relative energetic ordering of the AFI, AFII, and spin-restricted (spin-unpolarized or paramagnetic) phases of NiO using the four functionals described in the main text. All functionals correctly place the AFII configuration as the lowest-energy configuration.

Interestingly, both PBE and PBEsol make the AFI and paramagnetic configurations degenerate at shorter lattice constants, and nearly-degenerate near equilibrium. Both SCAN and r^{2}SCAN place the paramagnetic configuration much higher in energy than AFI, but place the AFI configuration much closer in energy to the AFII configuration than either PBE or PBEsol. However, neither find the AFI and AFII configurations to be nearly degenerate, save at lattice constants longer than those considered in our calculations.
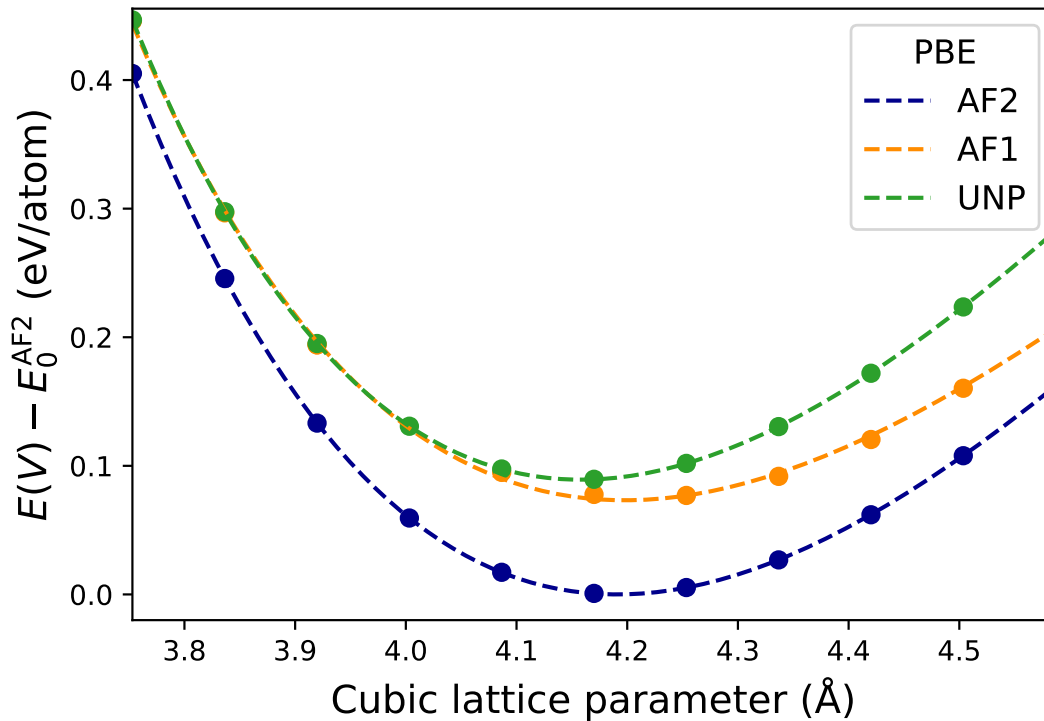
FIG. S8. Relative ordering of the AFI, AFII, and spin-restricted (UNP) phases of NiO, using PBE. All energies are plotted relative to the extrapolated energy minimum of the AFII configuration, which is experimentally determined to be the ground-state.
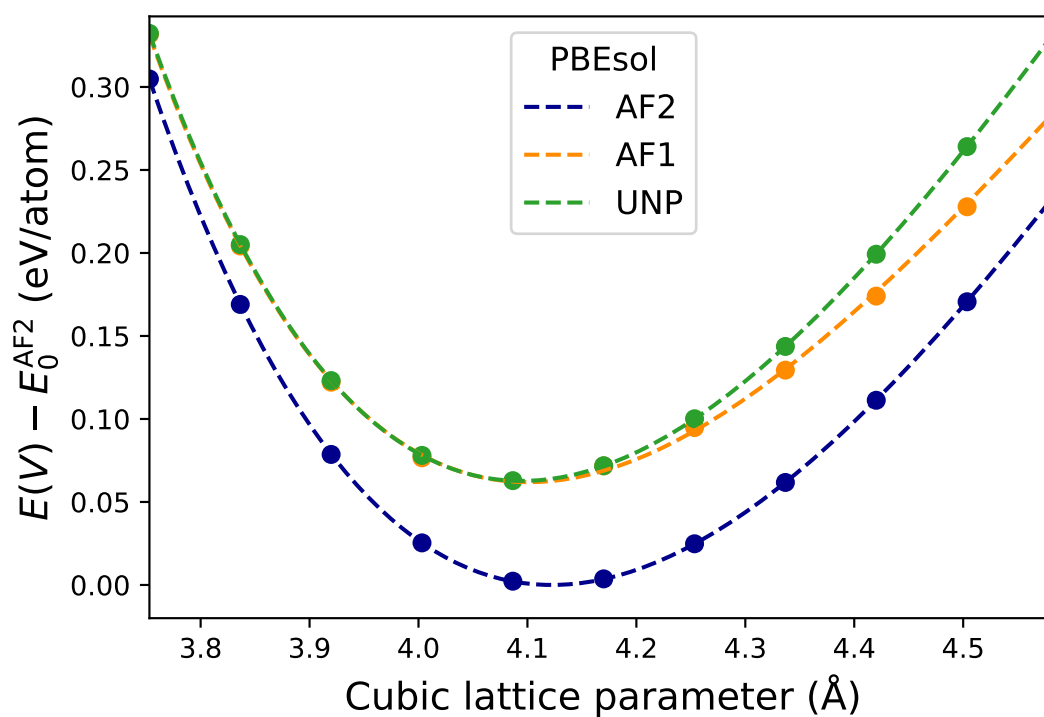
FIG. S9. Same as Fig. S8, but using PBEsol.
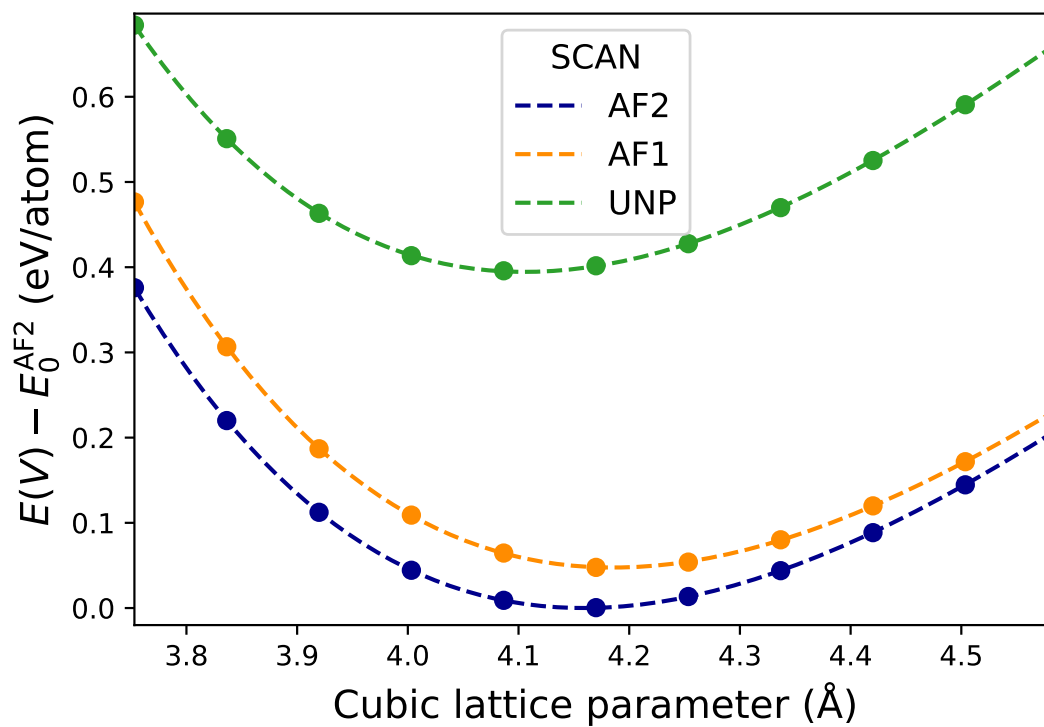
FIG. S10. Same as Fig. S8, but using SCAN.
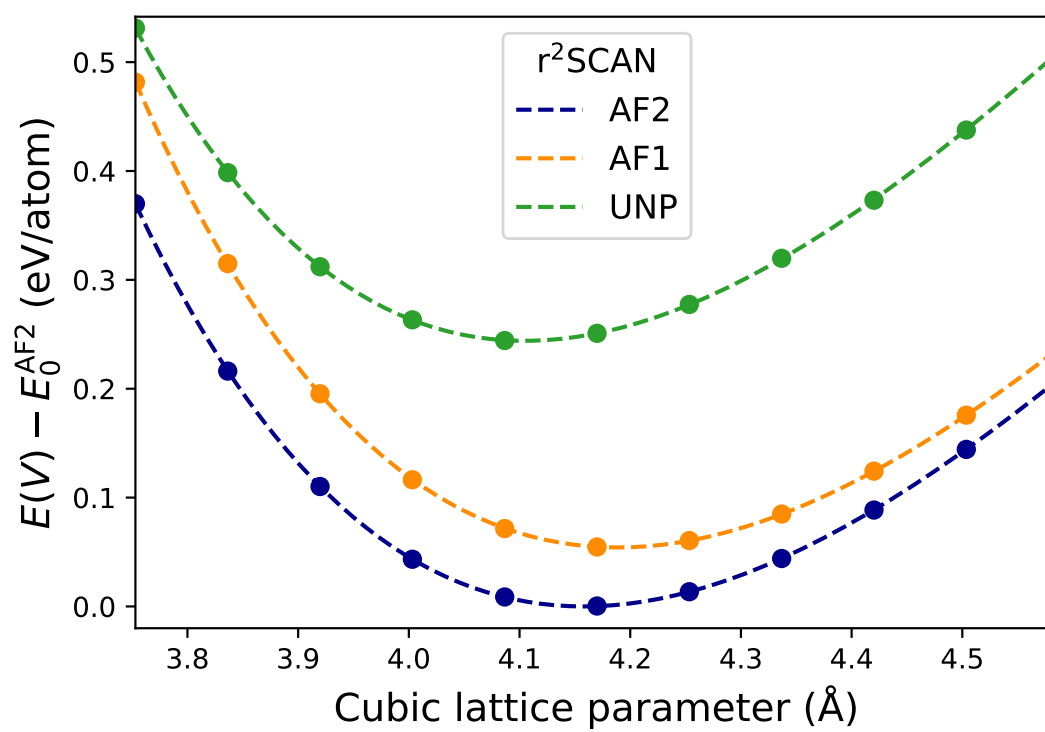
FIG. S11. Same as Fig. S8, but using r^2SCAN.

S9. MAGNETIC MOMENTS OF NIO AS A FUNCTION OF LATTICE CONSTANT

Figures S12 and S13 plot the absolute magnetic moment of a formula unit of NiO in the AFI and AFII configurations respectively. In both plots, the absolute magnetic moment on one Ni atom and the absolute magnetic moment on one O atom are summed and plotted. Note that in Figure S12 there is a slight dip in the magnetization predicted by r^2SCAN. This defect in the predictions is due to the fact that, for this lattice constant only, the net magnetization of the system is nonzero. It's not entirely clear why this occurs, though the smearing contribution to the energy does begin to increase for the smallest lattice constants. While the smearing contribution remains small (<1 meV/atom), this may indicate that increased occupation of states in the conduction band are causing issues with the wavefunction optimization in this case. Note however that this is the only calculation where this error occurs.
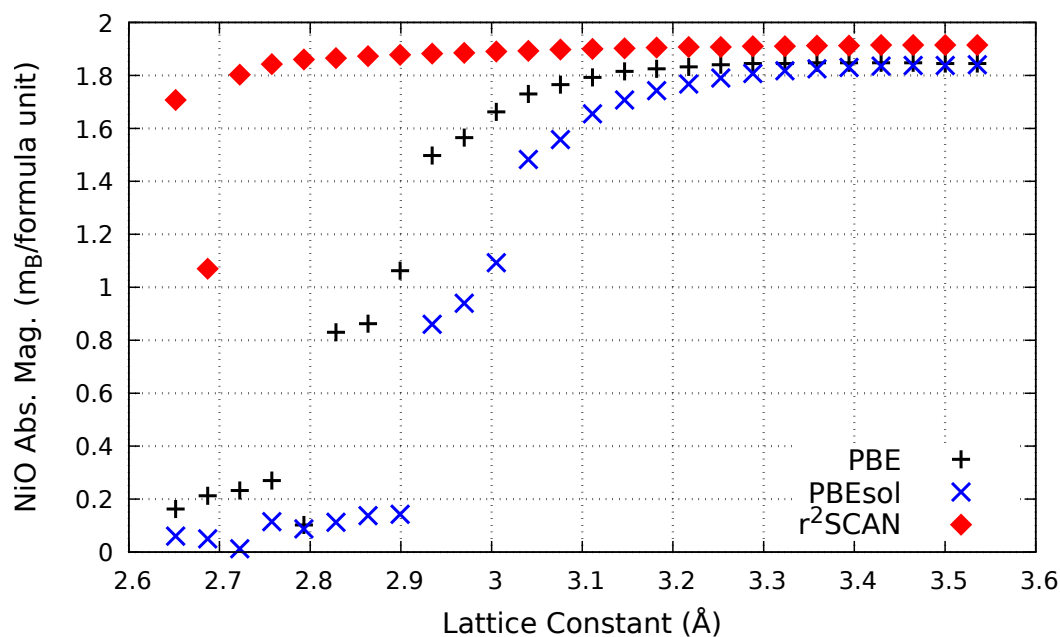
FIG. S12. Absolute magnetic moment on a formula unit of AFI NiO, in units of the Bohr magneton μ_B.
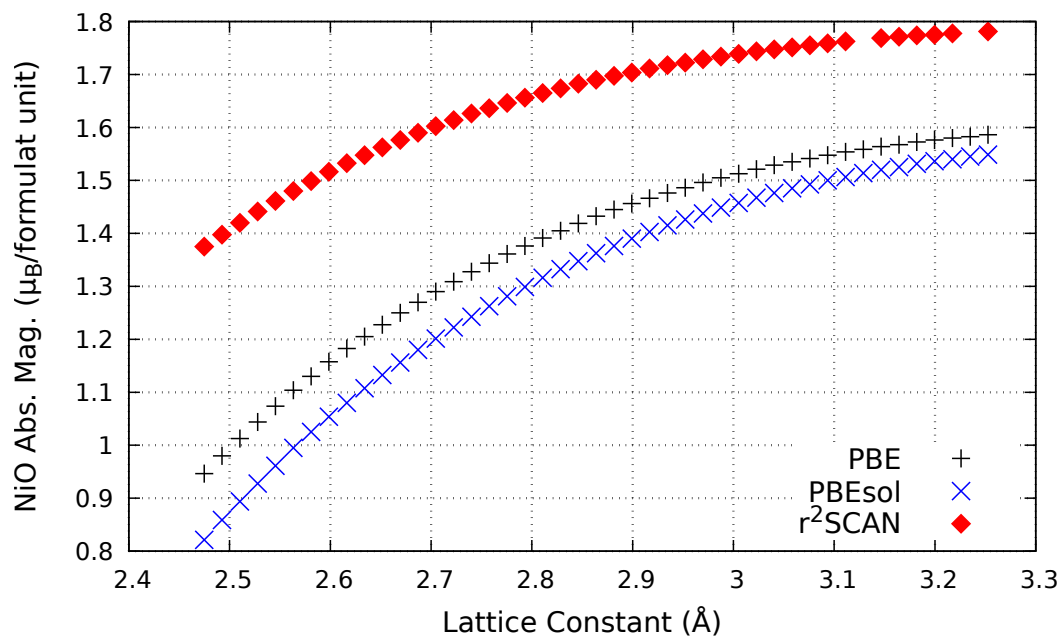
FIG. S13. Absolute magnetic moment on a formula unit of AFII NiO, in units of the Bohr magneton μ_B.

S10. HYBRID BAND GAPS, BAND EDGES, AND MAGNETIC MOMENTS FOR AFI NIO

This section presents figures that are analogous to Figs. 3 and 4 of the main text, but for the AFI configuration of NiO, rather than the AFII configuration.
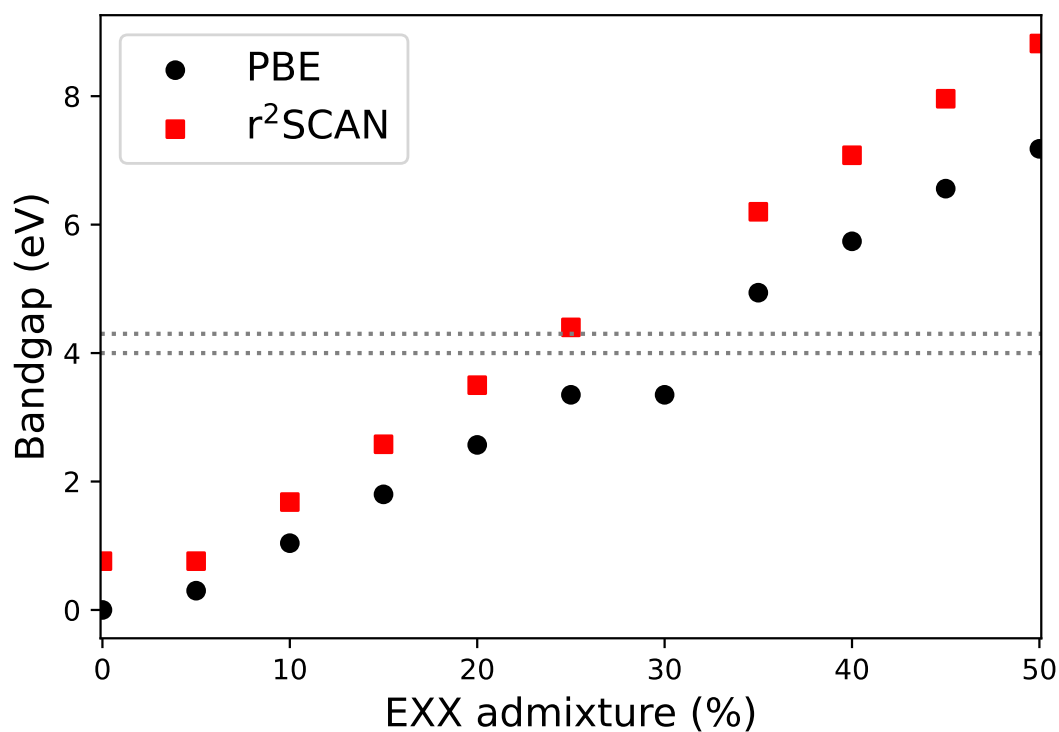
FIG. S14. Bandgap (eV) of AFI NiO as a function of exact exchange admixture in the global hybrids of PBE and r^2SCAN. All bandgaps were computed from the density of states. The dotted gray horizontal lines are experimental estimates of the bandgap, 4.0 and 4.3 eV[8]. This figure is analogous to Fig. 3(a) of the main text. The 30% r^2SCAN global hybrid data point is excluded because repeated attempts of the calculation failed to converge.
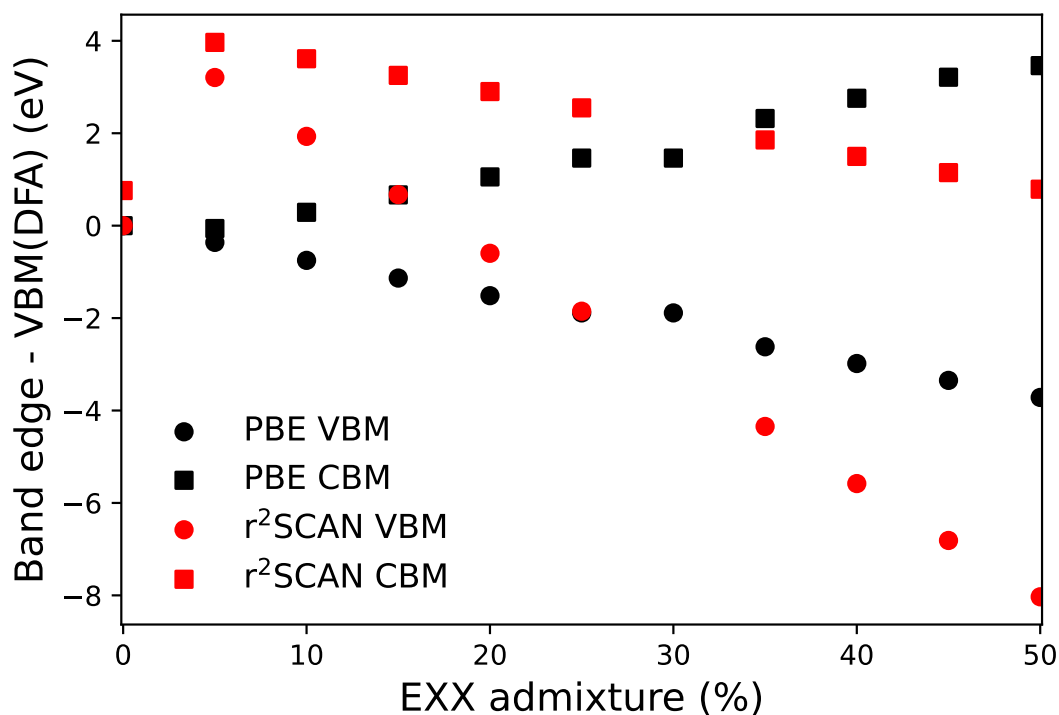
FIG. S15. Band edges (eV) of AFI NiO as a function of exact exchange admixture in the global hybrids of PBE and r^2SCAN. This figure is analogous to Fig. 3(b) of the main text. The 30% r^2SCAN global hybrid data point is excluded because repeated attempts of the calculation failed to converge.
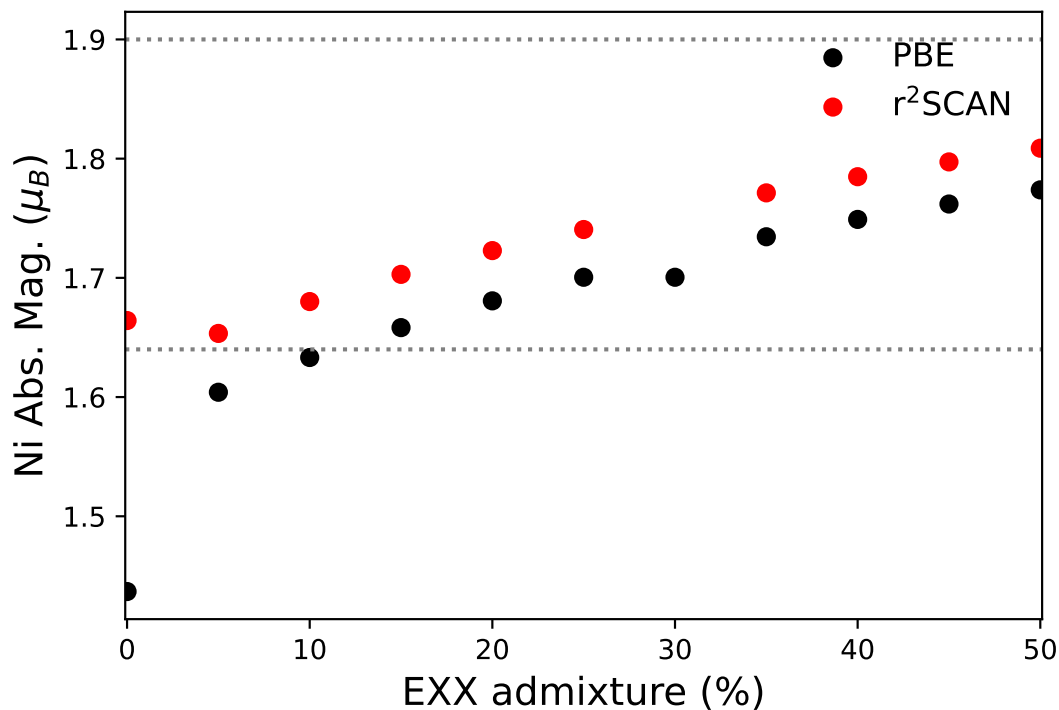
FIG. S16. Magnetic moment (μ_B) on an Ni atom in AFI NiO as a function of exact exchange admixture. This figure is analogous to Fig. 4 of the main text. Dotted horizontal lines are experimental estimates of the magnetic moment in NiO, 1.64 and 1.90 μ_B[8]. The 30% r^2SCAN global hybrid data point is excluded because repeated attempts of the calculation failed to converge.
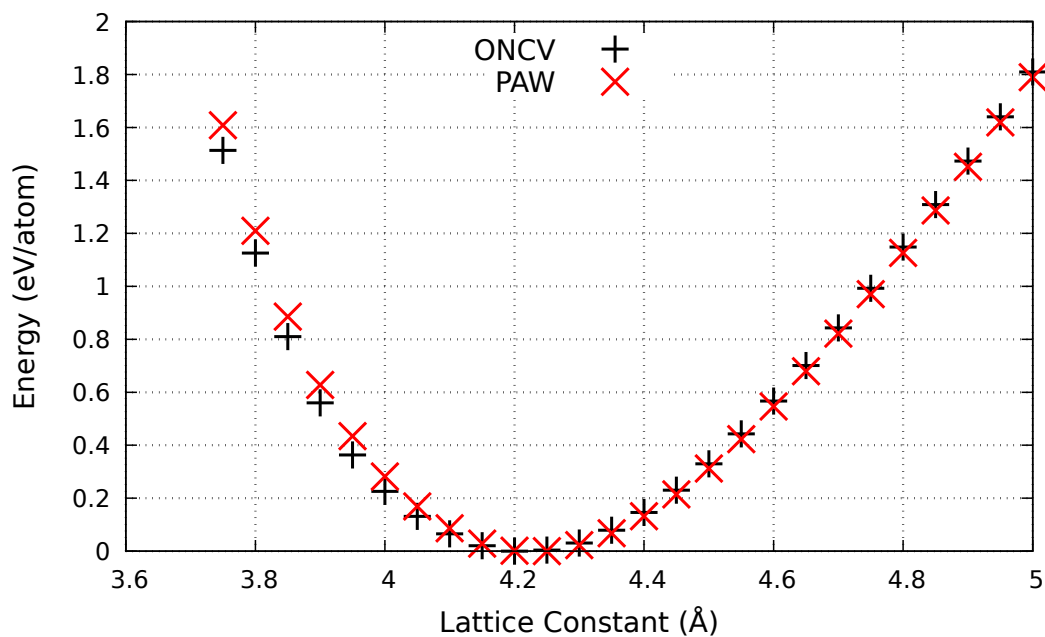
FIG. S17. Energy as a function of the cubic lattice constant of AFI NiO computed using the PBE pseudopotential with ONCV norm conserving pseudopoentials and PAW pseudopotentials. While there are slight discrepancies for large deviations from the minimum energy state, overall there is very close agreement.
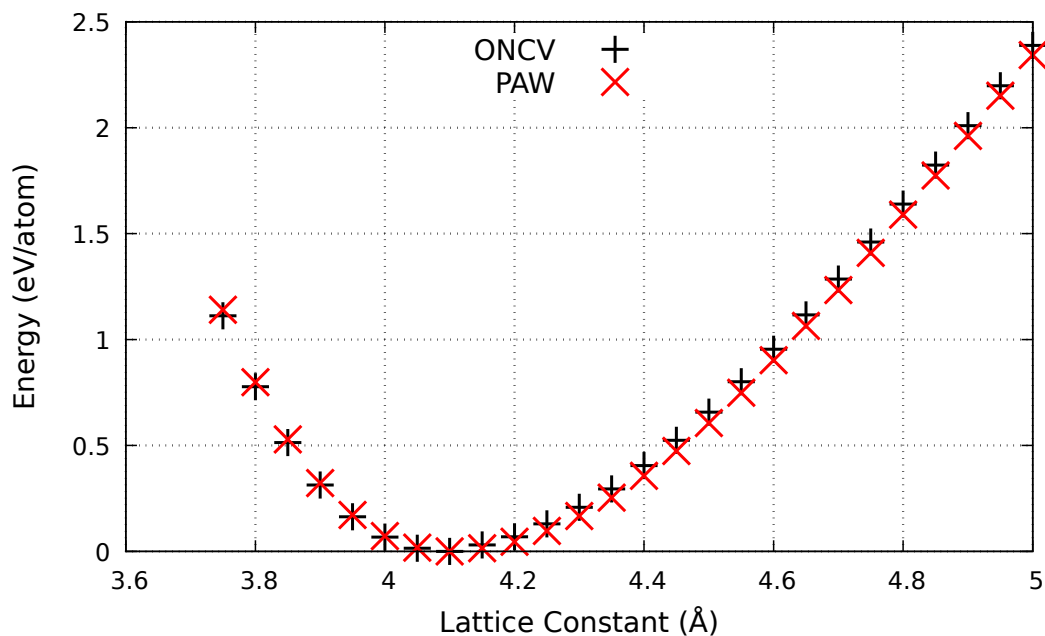
FIG. S18. Energy as a function of the cubic lattice constant of AFI NiO computed using the PBEsol pseudopotential with ONCV norm conserving pseudopoentials and PAW pseudopotentials. While there are slight discrepancies for large deviations from the minimum energy state, overall there is very close agreement.

S11. VISUALIZING THE MAGNETIC CONFIGURATIONS OF NIO

(a) AFI NiO.

(b) AFII NiO.
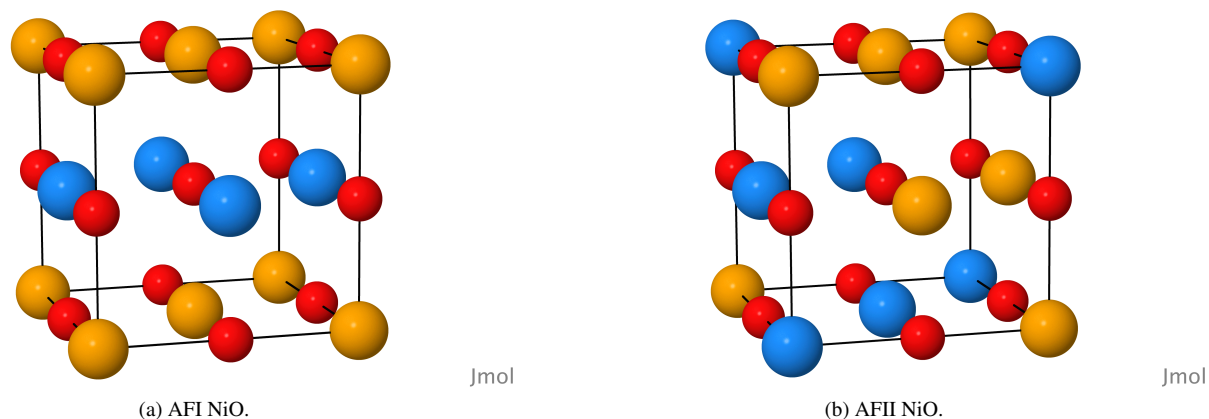
FIG. S19. Conventional cubic unit cell of NiO in the (a) AFI and (b) AFII configurations. Up-spin Ni atoms are colored orange, down-spin Ni atoms are colored blue, and O atoms are red. Both figures were generated with Jmol[44].

[1] M. A. Peña and J. L. G. Fierro, "Chemical structures and performance of perovskite oxides," Chem. Rev. **101**, 1981–2018 (2001).

[2] R. B. Comizzoli, R. P. Frankenthal, P. C. Milner, and J. D. Sinclair, "Corrosion of electronic materials and devices," Science **234**, 340–345 (1986).

[3] N. Basavegowda, K. Mishra, and Y. R. Lee, "Synthesis, characterization, and catalytic applications of hematite (α-Fe_2O_3) nanoparticles as reusable nanocatalyst," Adv. Nat. Sci: Nanosci. Nanotechnol. **8**, 025017 (2017).

[4] M. Pelaez, N. T. Nolan, S. C. Pillai, M. K. Seery, P. Falaras, A. G. Kontos, P. S. Dunlop, J. W. Hamilton, J. Byrne, K. O'Shea, M. H. Entezari, and D. D. Dionysiou, "A review on the visible light active titanium dioxide photocatalysts for environmental applications," Appl. Catal. B: Environ. **125**, 331–349 (2012).

[5] J. C. Védrine, "Heterogeneous catalysis on metal oxides," Catalysts **7**, 341 (2017).

[6] H. Peng and J. P. Perdew, "Synergy of van der Waals and self-interaction corrections in transition metal monoxides," Phys. Rev. B **96**, 100101 (2017).

[7] I. de P. R. Moreira, F. Illas, and R. L. Martin, "Effect of fock exchange on the electronic structure and magnetic coupling in nio," Phys. Rev. B **65**, 155102 (2002).

[8] F. Tran, P. Blaha, K. Schwarz, and P. Novák, "Hybrid exchange-correlation energy functionals for strongly correlated electrons: Applications to transition-metal monoxides," Phys. Rev. B **74**, 155108 (2006).

[9] C. Rödl, F. Fuchs, J. Furthmüller, and F. Bechstedt, "Quasiparticle band structures of the antiferromagnetic transition-metal oxides MnO, FeO, CoO, and NiO," Phys. Rev. B **79**, 235114 (2009).

[10] J. Sun, A. Ruzsinszky, and J. P. Perdew, "Strongly constrained and appropriately normed semilocal density functional," Phys. Rev. Lett. **115**, 036402 (2015).

[11] J. G. Brandenburg, J. E. Bates, J. Sun, and J. P. Perdew, "Benchmark tests of a strongly constrained semilocal functional with a long-range dispersion correction," Phys. Rev. B **94**, 115144 (2016).

[12] G. Sai Gautam and E. A. Carter, "Evaluating transition metal oxides within DFT-SCAN and SCAN + U frameworks for solar thermochemical applications," Phys. Rev. Mater. **2**, 095401 (2018).

[13] O. Y. Long, G. Sai Gautam, and E. A. Carter, "Evaluating optimal U for $3d$ transition-metal oxides within the SCAN+U framework," Physical Review Materials **4**, 045401 (2020), publisher: American Physical Society.

[14] Z.-h. Yang, H. Peng, J. Sun, and J. P. Perdew, "More realistic band gaps from meta-generalized gradient approximations: Only in a generalized Kohn-Sham scheme," Phys. Rev. B **93**, 205205 (2016).

[15] Y. Yamamoto, C. M. Diaz, L. Basurto, K. A. Jackson, T. Baruah, and R. R. Zope, "Fermi-Löwdin orbital self-interaction correction using the strongly constrained and appropriately normed meta-GGA functional," J. Chem. Phys. **151**, 154105 (2019).

[16] A. P. Bartók and J. R. Yates, "Regularized SCAN functional," J. Chem. Phys. **150**, 161101 (2019).

[17] J. W. Furness, A. D. Kaplan, J. Ning, J. P. Perdew, and J. Sun, "Accurate and numerically efficient r²SCAN meta-generalized gradient approximation," J. Phys. Chem. Lett. **11**, 8208–8215 (2020), correction, *ibid.* **11**, 9248 (2020).

[18] G. Trimarchi, Z. Wang, and A. Zunger, "Polymorphous band structure model of gapping in the antiferromagnetic and paramagnetic phases of the Mott insulators MnO, FeO, CoO, and NiO," Phys. Rev. B **97**, 035107 (2018).

[19] S. Choi, A. Kutepov, K. Haule, M. van Schilfgaarde, and G. Kotliar, "First-principles treatment of mott insulators: linearized qsgw+dmft approach," npj Quant. Mater. **1**, 16001 (2016).

[20] Y. Zhang, J. Furness, R. Zhang, Z. Wang, A. Zunger, and J. Sun, "Symmetry-breaking polymorphous descriptions for correlated materials without interelectronic U," Phys. Rev. B **102**, 045112 (2020).

[21] V. Potapkin, L. Dubrovinsky, I. Sergueev, M. Ekholm, I. Kantor, D. Bessas, E. Bykova, V. Prakapenka, R. P. Hermann, R. Rüffer, V. Cerantola, H. J. M. Jönsson, W. Olovsson, S. Mankovsky, H. Ebert, and I. A. Abrikosov, "Magnetic interactions in nio at ultrahigh pressure," Phys. Rev. B **93**, 201110 (2016).

[22] J. P. Perdew, K. Burke, and M. Ernzerhof, "Generalized gradient approximation made simple," Phys. Rev. Lett. **77**, 3865 (1996).

[23] J. P. Perdew, A. Ruzsinszky, G. I. Csonka, O. A. Vydrov, G. E. Scuseria, L. A. Constantin, X. Zhou, and K. Burke, "Restoring the density-gradient expansion for exchange in solids and surfaces," Phys. Rev. Lett. **100**, 136406 (2008).

[24] S. Swathilakshmi, R. Devi, and G. S. Gautam, "Performance of the r²SCAN functional in transition metal oxides," (2023), arXiv:2301.00535.

[25] P. Giannozzi, S. Baroni, N. Bonini, M. Calandra, R. Car, C. Cavazzoni, D. Ceresoli, G. L. Chiarotti, M. Cococcioni, I. Dabo, A. D. Corso, S. de Gironcoli, S. Fabris, G. Fratesi, R. Gebauer, U. Gerstmann, C. Gougoussis, A. Kokalj, M. Lazzeri, L. Martin-Samos, N. Marzari, F. Mauri, R. Mazzarello, S. Paolini,

A. Pasquarello, L. Paulatto, C. Sbraccia, S. Scandolo, G. Sclauzero, A. P. Seitsonen, A. Smogunov, P. Umari, and R. M. Wentzcovitch, "QUANTUM ESPRESSO: a modular and open-source software project for quantum simulations of materials," J. Phys. Condens. Matter **21**, 395502 (2009).

[26] P. Giannozzi, O. Andreussi, T. Brumme, O. Bunau, M. B. Nardelli, M. Calandra, R. Car, C. Cavazzoni, D. Ceresoli, M. Cococcioni, N. Colonna, I. Carnimeo, A. D. Corso, S. de Gironcoli, P. Delugas, R. A. DiStasio, A. Ferretti, A. Floris, G. Fratesi, G. Fugallo, R. Gebauer, U. Gerstmann, F. Giustino, T. Gorni, J. Jia, M. Kawamura, H.-Y. Ko, A. Kokalj, E. Küçükbenli, M. Lazzeri, M. Marsili, N. Marzari, F. Mauri, N. L. Nguyen, H.-V. Nguyen, A. O. de-la Roza, L. Paulatto, S. Poncé, D. Rocca, R. Sabatini, B. Santra, M. Schlipf, A. P. Seitsonen, A. Smogunov, I. Timrov, T. Thonhauser, P. Umari, N. Vast, X. Wu, and S. Baroni, "Advanced capabilities for materials modelling with Quantum ESPRESSO," J. Phys. Condens. Matter **29**, 465901 (2017).

[27] S. Lehtola, C. Steigemann, M. J. Oliveira, and M. A. Marques, "Recent developments in LIBXC — a comprehensive library of functionals for density functional theory," SoftwareX **7**, 1–5 (2018).

[28] D. Vanderbilt, "Optimally smooth norm-conserving pseudopotentials," Phys. Rev. B **32**, 8412–8415 (1985).

[29] M. Schlipf and F. Gygi, "Optimization algorithm for the generation of oncv pseudopotentials," Computer Phys. Commun. **196**, 36–44 (2015).

[30] W. L. Roth and G. A. Slack, "Antiferromagnetic structure and domains in single crystal nio," J. Appl. Phys. **31**, S352–S353 (1960).

[31] A. Schrön, C. Rödl, and F. Bechstedt, "Energetic stability and magnetic properties of MnO in the rocksalt, wurtzite, and zinc-blende structures: Influence of exchange and correlation," Phys. Rev. B **82**, 165109 (2010).

[32] A. B. Alchagirov, J. P. Perdew, J. C. Boettger, R. C. Albers, and C. Fiolhais, "Energy and pressure versus volume: Equations of state motivated by the stabilized jellium model," Phys. Rev. B **63**, 2241151–22411516 (2001).

[33] A. D. Kaplan and J. P. Perdew, "Laplacian-level meta-generalized gradient approximation for solid and liquid metals," Phys. Rev. Materials **6**, 083803 (2022).

[34] X.-B. Feng and N. M. Harrison, "Metal-insulator and magnetic transition of NiO at high pressures," Physical Review B **69**, 035114 (2004), publisher: American Physical Society.

[35] D. Hait and M. Head-Gordon, "How accurate is density functional theory at predicting dipole moments? An assessment using a new database of 200 benchmark values," J. Chem. Theory Comput. **14**, 1969–1981 (2018).

[36] M. DelloStritto, J. Xu, X. Wu, and M. L. Klein, "Aqueous solvation of the chloride ion revisited with density functional theory: impact of correlation and exchange approximations," Phys. Chem. Chem. Phys. **22**, 10666–10675 (2020).

[37] J. P. Perdew, W. Yang, K. Burke, Z. Yang, E. K. Gross, M. Scheffler, G. E. Scuseria, T. M. Henderson, I. Y. Zhang, A. Ruzsinszky, H. Peng, J. Sun, E. Trushin, and A. Görling, "Understanding band gaps of solids in generalized Kohn-Sham theory," Proc. Nat. Acad. Sci. U.S.A. **114**, 2801–2806 (2017).

[38] N. M. Harrison, V. R. Saunders, R. Dovesi, W. C. Mackrodt, A. S. Alexandrov, C. N. R. Rao, J. N. Murrell, R. L. Johnston, and D. E. Logan, "Transition Metal Materials: A First Principles Approach to the Electronic Structure of the Insulating Phase [and Discussion]," Philosophical Transactions: Mathematical, Physical and Engineering Sciences **356**, 75–88 (1998), publisher: The Royal Society.

[39] M. D. Towler, N. L. Allan, N. M. Harrison, V. R. Saunders, W. C. Mackrodt, and E. Aprà, "Ab initio study of MnO and NiO," Physical Review B **50**, 5041–5054 (1994), publisher: American Physical Society.

[40] J. Muscat, A. Wander, and N. M. Harrison, "On the prediction of band gaps from hybrid functional theory," Chemical Physics Letters **342**, 397–401 (2001).

[41] L. Zhang, J. Han, H. Wang, R. Car, and W. E, "Deep potential molecular dynamics: A scalable model with the accuracy of quantum mechanics," Phys. Rev. Lett. **120**, 143001 (2018).

[42] C. Malosso, L. Zhang, R. Car, S. Baroni, and D. Tisi, "Viscosity in water from first-principles and deep-neural-network simulations," npj Comput. Mater. **8**, 139 (2022).

[43] C. R. Harris, K. J. Millman, S. J. van der Walt, R. Gommers, P. Virtanen, D. Cournapeau, E. Wieser, J. Taylor, S. Berg, N. J. Smith, R. Kern, M. Picus, S. Hoyer, M. H. van Kerkwijk, M. Brett, A. Haldane, J. F. del Río, M. Wiebe, P. Peterson, P. Gérard-Marchant, K. Sheppard, T. Reddy, W. Weckesser, H. Abbasi, C. Gohlke, and T. E. Oliphant, "Array programming with NumPy," Nature **585**, 357–362 (2020).

[44] R. M. Hanson, J. Prilusky, Z. Renjian, T. Nakane, and J. L. Sussman, "JSmol and the Next-Generation Web-Based Representation of 3D Molecular Structure as Applied to Proteopedia," Isr. J. Chem. **53**, 207–216 (2013).